Acta Mechanica 123, 117–133 (1997)

ACTA MECHANICA

Instability of plane compressible gas sheets

X. Li and **A. Bhunia,** Victoria, British Columbia

(Received April 23, 1996)

Summary. The instability of a plane compressible gas sheet in a quiescent viscous liquid medium of infinite expanse has been studied. It is found that there exist two unstable modes of disturbances, sinuous and varicose. For temporal instability, sinuous disturbance is stable if the gas Weber number, defined as the ratio of aerodynamic to capillary forces, is less than unity, varicose mode controls the instability process except for large Weber numbers when both modes become equally important, and gas compressibility effect always enhances instability development and induces an additional range of unstable wave numbers. For spatial-temporal evolution of disturbances, it is found that convective instability does not exist at all and the instability of plane gas sheets is always absolute in nature, which is strikingly opposite to the instability of plane liquid sheets. The absolutely unstable disturbance is found always temporally growing, although it may be spatially growing or decaying depending on flow conditions. Gas compressibility always enhances and liquid viscosity damps out both the temporal and the spatial part of absolute instability growth rate. Although the Weber number always promotes the temporal growth rate of absolute instability, it has a dual effect of enhancing and inhibiting the spatial growth rate.

1 Introduction

Bubbles from the disintegration of gas jets and sheets are of fundamental importance in many practical and industrial applications. Instability and disintegration of gas sheets are conveniently utilized in various chemical and pharmaceutical industries for gas dissolution in a liquid medium [1], in mining industries for coal and mineral preparation by froth floatation technique [2], [3] and in bubble plumes widely used for aeration, protection of structures against ocean waves and for mixing of stratified reservoirs [4]. The sizes of bubbles, generated by the disintegration of a continuous gas sheet, are important factors contributing to the effectiveness and efficiency of many industrial operations involving bubble formation. A sound knowledge of the gas sheet instability and disintegration process is thus essential for the control of bubble formation and gas dissolution processes. Although extensive studies have been carried out on structure and mean flow of bubble plumes formed by round jets and two dimensional gas sheets [5]–[7], little attention has been paid to the instability of gas sheets and jets preceeding the formation of bubbles.

However, a similar problem, the instability of plane liquid sheets in a gas medium, has been widely investigated in connection with liquid atomization and sprays used in power generation and propulsion systems [8]–[10] and spray drying operations [11]. Squire [12], York, Stubbs and Tek [13] and Hagerty and Shea [14] studied the temporal instability of a plane inviscid liquid sheet in a surrounding inviscid gas medium, and Li and Tankin [15] analyzed the temporal instability of plane viscous liquid sheets. According to the causality condition of Briggs [16] and Bers [17], Lin, Lian and Creighton [18] studied the absolute and convective instability of a viscous liquid sheet in a stationary gas medium. They reported that the sinuous mode of disturbance is

neutrally stable below a critical liquid Weber number of one and in the sense of Briggs [16] and Bers [17] they termed it as pseudo-absolute instability. They also concluded that for sinuous mode at liquid Weber numbers higher than the critical value of one and for varicose mode at any Weber number, convective instability exists for a non-zero gas density. Li [19] further investigated the spatial instability of plane liquid sheets and found that liquid viscosity has both a stabilizing and a destabilizing effect for sinuous mode at low Weber numbers, while for varicose mode and sinuous mode at higher Weber numbers, it is always stabilizing. The same problem has also been addressed by Ibrahim [20] and the subject has been reviewed by Li [21].

Recently, Li and Bhunia investigated the temporal instability of an incompressible plane gas sheet [22]–[23]. It was found that there exist two unstable modes of disturbances, sinuous and varicose, and surface tension always reduces, while the relative velocity between the gas and liquid phases and the gas density always enhance instability development. For both unstable modes, the presence of liquid viscosity increases the instability limit, which is however independent of the absolute value of viscosity. It was also shown that the sinuous mode becomes stable when the gas Weber number, defined as the ratio of aerodynamic forces to surface tension forces, is less than the critical value of one. At slightly larger gas Weber numbers, liquid viscosity exhibits dual effects – it may enhance or suppress the growth of unstable disturbances, depending on specific flow conditions. However, for sinuous mode at high Weber numbers and varicose mode at any Weber numbers, liquid viscosity always reduces disturbances growth rates and dominant wave numbers. Unlike the case for plane liquid sheets, varicose mode controls the instability process for all Weber number ranges and for both inviscid and viscous liquids, and only at high Weber numbers varicose and sinuous modes become almost equally important. It was further found that the wave velocity for both unstable modes is much smaller than the gas velocity at the mode of maximum instability, implying that in practice the disturbance waves appear almost stationary rather than travelling-wave type, in contrast with the plane liquid sheet results.

The present work reports the subsequent study on the temporal, absolute and convective instability of a two-dimensional compressible gas sheet in a viscous liquid medium and the effects of various physical parameters, such as surface tension, gas density, liquid viscosity and gas compressibility, on the instability process. The analysis shows that the sinuous mode is neutrally stable below a critical value of gas Weber number, which is always constant at one. Varicose mode dominates the instability process, although at large gas Weber numbers both modes become equally important. Strikingly opposite to the plane liquid sheet case, the spatial-temporal evolution of disturbances is always absolute in nature for plane gas sheets, and convective instability does not exist at all. A linear stability analysis is formulated and dispersion relations are derived in the next Section. These dispersion relations are then solved numerically to obtain gas sheet instability characteristics which are presented subsequently.

2 Instability analysis

A two-dimensional, inviscid, compressible gas sheet of uniform thickness $2a$ and density $\bar{\varrho}_g$ is injected with a uniform constant velocity U_g into a quiescent liquid medium of infinite expanse. The liquid medium has a density $\bar{\varrho}_l$ and dynamic viscosity μ_l. The effect of gravity and liquid compressibility is neglected. The neglect of gas viscosity is based on the observation that the viscosity of the gas is only weakly stabilizing and does not influence the relevant phenomenon appreciably, as Lin and Ibrahim [24] found in a related work.

The base flow field is given by, for the gas phase, a constant velocity U_g in the direction of flow, a constant pressure P_g and a constant density $\bar{\varrho}_g$, and for the liquid phase, a zero velocity in all directions and a constant pressure P_l. Further, $P_g = P_l$ from the continuity of normal stresses across the gas-liquid interfaces. On this base flow are superimposed fluctuations in velocity, pressure and gas density, denoted as $\mathbf{u}_j = (u_j, v_j) = \mathbf{u}_j(x, y, t)$, $p_j = p_j(x, y, t)$ and $\varrho_g = \varrho_g(x, y, t)$, respectively. Here the subscript $j =$ "g" represents the quantities related to the gas phase and $j =$ "l" to the liquid phase. The corresponding disturbed gas-liquid interfaces are illustrated in Fig. 1, and represented by $y = \pm a + \xi_\pm$ for the upper and lower interface, respectively.

Equations governing the perturbed flow are the conservation of mass and momentum along with an equation of state for the gas phase. They are, after linearization

$$\delta_j\left(\frac{\partial}{\partial t} + U_g\frac{\partial}{\partial x}\right)\varrho_j + \bar{\varrho}_j(\nabla\cdot\mathbf{u}_j) = 0, \tag{1}$$

$$\frac{\partial \mathbf{u}_j}{\partial t} + \delta_j U_g\frac{\partial \mathbf{u}_j}{\partial x} = -\frac{1}{\bar{\varrho}_j}\nabla p_j + (1-\delta_j)\,\nu_l\nabla^2\mathbf{u}_j, \tag{2}$$

$$p_g = \left(\frac{\partial p_g}{\partial \varrho_g}\right)_s \varrho_g = c^2\varrho_g \tag{3}$$

where $\delta_j = 1$ for $j = g$ and 0 for $j = l$, ν_l is the kinematic viscosity of the liquid, the subscript "s" denotes isentropic process and c is the velocity of sound in the gas medium and is a constant. The kinematic and dynamic boundary conditions apply at the liquid-gas interfaces as follows:

$$v_j = \frac{\partial \xi_\pm}{\partial t} + \delta_j U_g\frac{\partial \xi_\pm}{\partial x} \quad \text{at} \quad y \approx \pm a, \tag{4}$$

$$(\tau_{yy})_g - (\tau_{yy})_l = P_l - 2\mu_l\frac{\partial v_l}{\partial y} - P_g = \pm\sigma\frac{d^2\xi_\pm}{dx^2} \quad \text{at} \quad y \approx \pm a, \tag{5}$$

$$(\tau_{xy})_l = \mu_l\left(\frac{\partial u_l}{\partial y} + \frac{\partial v_l}{\partial x}\right) = 0 \quad \text{at} \quad y \approx \pm a. \tag{6}$$

A normal mode solution to the governing equations is sought in the following form:

$$[p_g, v_g, \psi_l, \xi_+, \xi_-] = [\tilde{p}_g(y), \tilde{v}_g(y), \Psi_l(y), \xi_0, \xi_0 e^{i\theta}]\, e^{i(kx-\omega t)} \tag{7}$$

where ψ_l is the stream function for the liquid phase, ξ_0 is the initial disturbance amplitude and θ is the phase angle difference between the two surface waves at the upper and lower interfaces, as shown in Fig. 1. Then the bounded solution to the governing equations subjected to the above boundary conditions yields, in dimensionless form, either

$$\frac{(m-\Omega)^2}{r}\tanh(rm) + \frac{\Omega^2}{\varrho} + \frac{4}{\varrho\,\mathrm{Re}}m^2 i\Omega - \frac{4}{\varrho\,\mathrm{Re}^2}m^3(m-n) - \frac{m^3}{\mathrm{We}_g} = 0 \quad (\text{for } \theta = 0) \tag{8}$$

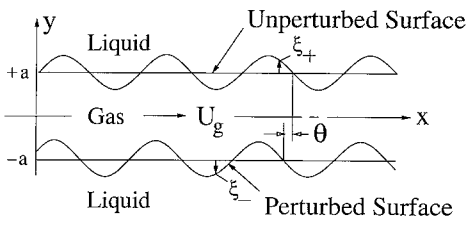

Fig. 1. Schematic of a plane gas sheet and surface waves

or

$$\frac{(m-\Omega)^2}{r}\coth(rm)+\frac{\Omega^2}{\varrho}+\frac{4}{\varrho\,\mathrm{Re}}m^2i\Omega-\frac{4}{\varrho\,\mathrm{Re}^2}m^3(m-n)-\frac{m^3}{\mathrm{We}_g}=0 \quad (\text{for } \theta=\pi) \tag{9}$$

where $m = ka$ is the dimensionless wavenumber, $\Omega = \omega a/U_g$ is the dimenionless wave frequency, $\mathrm{Re} = U_g a/\nu_l$ is the Reynolds number, $\mathrm{We}_g = \bar{\varrho}_g U_g{}^2 a/\sigma$ is the gas Weber number, $\varrho = \bar{\varrho}_g/\bar{\varrho}_l$ is the density ratio, $n = \sqrt{m^2 - i\,\mathrm{Re}\Omega}$, $r = \sqrt{m^2 - (m-\Omega)^2\,\mathrm{Ma}^2}/m$ and $\mathrm{Ma} = U_g/c$ is the Mach number. Clearly, when $\mathrm{Ma} = 0, r = 1$, Eqs. (8) and (9) then reduce to the dispersion relations for the incompressible gas sheets obtained earlier by Li and Bhunia [22]. It is also interesting to note that only two values of θ are possible, as given above in Eqs. (8) and (9). The case of $\theta = 0$ corresponds to waves at the upper and lower interfaces oscillating exactly in phase which are often called sinuous disturbance. Similarly the case of $\theta = \pi$ represents two interfacial waves displacd exactly out of phase, which are usually referred to as varicose disturbance.

3 Results and discussions

3.1 Temporal instability

In the dispersion relation, Eqs. (8) and (9), derived in the previous Section, if the wave number m is real and the imaginary part of the wave frequency Ω_i is positive for a certain mode of disturbance, the disturbance will grow exponentially with time and will eventually lead to the breakdown of the gas sheet. Various physical parameters influence the temporal instability of the gas sheet, they are surface tension, gas density and velocity, liquid density and viscosity and gas compressibility. Effects of all these parameters, except the gas compressibility, on the temporal instability have been investigated recently [22], [23]. Therefore, only the gas compressibility effect is considered in the present study. The gas compressibility effect is quantitatively expressed in terms of dimensionless Mach number and its effect on the instability characteristics will be investigated here.

3.1.1 Instability limit

The instability limit m_c, also often known as the cut-off wave number, is the maximum wavenumber of the disturbance causing instability. Hence, the instability limit can be obtained by setting $\Omega_i = 0$. For a compressible gas sheet, the instability limit m_c is determined by numerically solving the dispersion relations (8) and (9) for sinuous and varicose mode of disturbances, respectively. Figure 2 illustrates the typical variation of the instability limit with the Mach number, where the flow conditions are given by the density ratio $\varrho = 0.1$ and gas Weber number $\mathrm{We}_g = 3.0$. It is evident that for both the sinuous and the varicose mode of disturbances, the instability limit always increases with the Mach number for viscous and inviscid surrounding liquid. This implies that gas compressibility effect induces an additional range of wave numbers and corresponding wavelengths of disturbances for which the gas sheet is unstable, and the absolute value of this additional range depends on the degree of gas compressibility. It is further seen that at low Mach numbers the dependence of the instability limit on the Mach number is fairly weak, and the gas sheet can be considered essentially incompressible if the Mach number is less than approximately 0.3. Above this value, the instability limit increases rapidly with the Mach number.

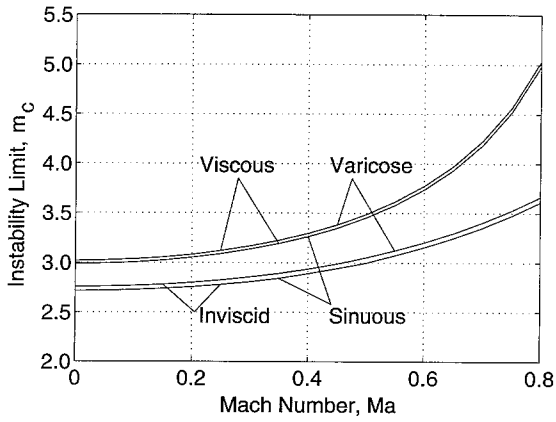

Fig. 2. Instability limit of sinuous and varicose mode for inviscid and viscous (Re = 10) surrounding liquids. $We_g = 3.0$ and $\varrho = 0.1$

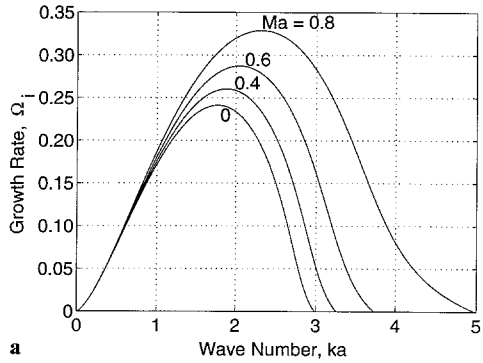

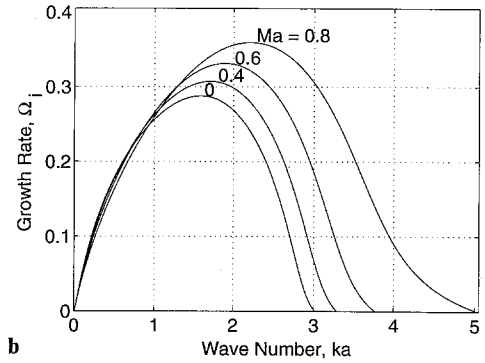

Fig. 3. Dimensionless growth rate vs. wave number for different Mach numbers. $\varrho = 0.1$, $We_g = 3.0$ and Re = 100. **a** Sinuous mode **b** varicose mode

Figure 2 also shows that at the given Weber number the varicose mode has a larger instability limit for both an inviscid and a viscous liquid at any Mach number. However, further numerical calculations indicate that at higher Weber numbers the instability limit for sinuous mode asymptotically approaches the same value as that for the varicose mode at all Mach number conditions.

Similar to the incompressible gas sheet, viscosity also broadens the instability limit for compressible gas sheets. For any values of the Mach number, there is an additional range of wave numbers for which the gas sheet is unstable only for viscous surrounding liquid, representing the viscosity-enhanced instability region [15], [22]. The inviscid and viscous curves in Fig. 2 further reveal that the range for the viscosity-enhanced instability broadens with the Mach number, especially at conditions close to the transonic flow.

3.1.2 Growth rate

Disturbance growth rate is determined by solving the dispersion relations, Eqs. (8) and (9), by using Muller's method [25]. The effect of gas compressibility on the disturbance growth rate is shown in Fig. 3 for the gas Weber number $We_g = 3.0$ and the density ratio $\varrho = 0.1$. It is clear from Fig. 3 that for sinuous mode the growth rate increases with the Mach number for any wavenumber, although at low wave numbers the increment is very small and hardly detectable. On the other hand, for varicose mode at low wave numbers the Mach number first enhances and then reduces the wave growth rate. At large wave numbers the growth rate for varicose mode always increases with the Mach number. It is also noted from Fig. 3 that the maximum growth rate, which eventually controls the instability process, always increases with the Mach number for both modes of disturbances along with the dominant and cut-off wavenumbers. Thus it can be concluded that the gas compressibility has an overall destabilizing effect on the plane gas sheet. This observation is valid for all conditions of the Weber number, the Reynolds number and the density ratio.

3.1.3 Maximum growth rate and dominant wave number

For temporal instability, the breakdown of a continuous gas sheet into a train of bubbles is usually considered to be dictated by the maximum growth rate and the corresponding wave number or wavelength of the disturbances. Figure 4 shows the variation of the maximum growth rate with the Mach number for a gas Weber number $We_g = 3.0$ and a density ratio $\varrho = 0.1$. It is evident that irrespective of the mode of disturbance and liquid viscosity, the maximum growth rate always increases with the Mach number as shown earlier, although at low Mach numbers

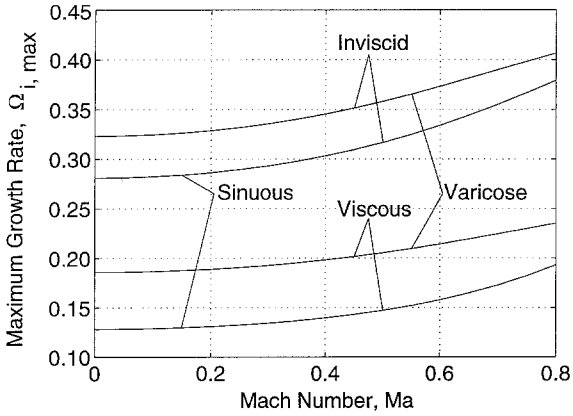

Fig. 4. Maximum growth rate of sinuous and varicose mode for inviscid and viscous (Re = 10) surrounding liquids. $We_g = 3.0$ and $\varrho = 0.1$

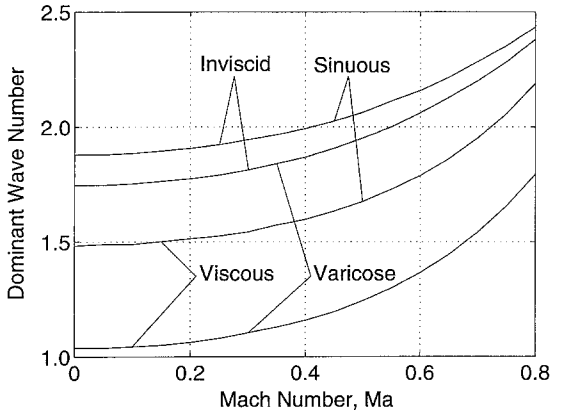

Fig. 5. Dominant wave number for sinuous and varicose mode for inviscid and viscous (Re = 10) surrounding liquids. $We_g = 3.0$ and $\varrho = 0.1$

(Ma $\leqq$ 0.3) the increment is small. Thus the gas sheet may be considered incompressible if Ma $\leqq$ 0.3. Comparing the inviscid and viscous results in Fig. 4, it becomes clear that a viscous effect always reduces the maximum growth rate for both sinuous and varicose modes of disturbances. It is also clear that at this condition of the gas Weber number ($We_g = 3$) varicose mode has a larger maximum growth rate than the corresponding sinuous mode at any Mach number and thus dictates the overall instability process. At any Mach number, further numerical calculations indicate that at higher Weber numbers the maximum growth rate for sinuous mode approaches, from below, that of varicose mode until they become almost equal and thus equally important in the instability process. It should be pointed out that Fig. 4 is representative of the Mach number effect on the maximum growth rate for any Weber numbers and density ratios.

The variation of the corresponding dominant wave number with the Mach number is shown in Fig. 5 for the same conditions as in Fig. 4. Clearly, the dominant wave number increases with the Mach number, indicating that gas compressibility effects shifts the mode of maximum instability to a disturbance of shorter wavelength. It is also evident that viscous effects reduce the dominant wave number for both modes of disturbances, and the reduction for varicose mode is far more than that for the corresponding sinuous mode. Although at the present condition of the Weber number sinuous mode has a larger dominant wave number than the varicose mode, it is found that at any Mach number the dominant wave number has a complex variation for the two types of disturbance waves depending on the value of the gas Weber number, as shown earlier by Li and Bhunia [22], [23] for the incompressible gas sheets.

3.1.4 Wave velocity

The dimensionless disturbance wave velocity, normalized by the gas sheet velocity U_g, is given by Ω_r/m, and the typical effect of the Mach number is shown in Fig. 6. It is clear that for both modes of disturbances the wave velocity is enhanced by the gas compressibility effect, although the effect

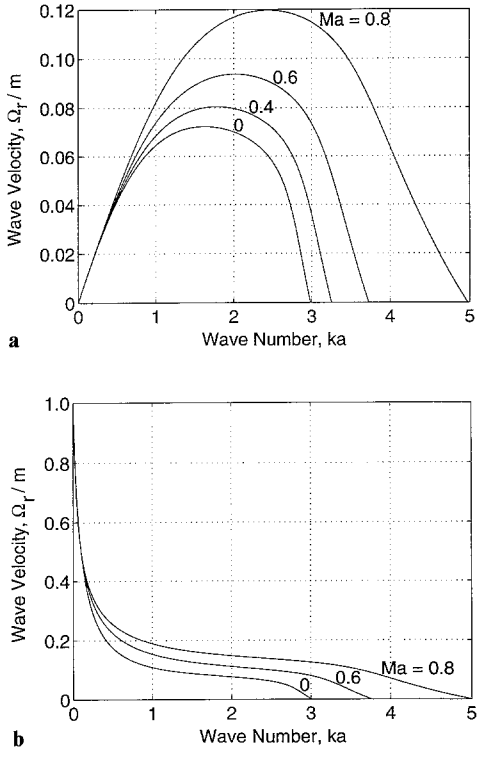

Fig. 6. Dimensionless wave velocity vs. wave number for different Mach numbers. $\varrho = 0.1$, $We_g = 3.0$ and Re = 100. **a** Sinuous mode, **b** varicose mode

is small at low wave numbers. The wave velocity for the sinuous mode vanishes at $m = 0$ and at the instability limit $m = m_c$, and it reaches the maximum value approximately at the dominant wave number range. On the other hand, the wave velocity for the varicose mode decreases rapidly and monotonically from the value of one at $m = 0$. Over a wide range of wave numbers including the dominant wave number, it is weakly dependent on the wave number until it finally decreases rapidly again to zero at the instability limit. Around the dominant wave numbers, the wave velocity for both modes is smaller than the gas sheet velocity, especially at low Mach numbers. However, the wave velocity of a compressible gas sheet is in general not negligible at the dominant wave numbers when compared with the gas sheet velocity, in contrast with the result for incompressible gas sheets [22]. With an increase in the Mach number, the wave velocity increases rapidly, especially close to the transonic flow region.

3.2 Absolute and convective instability

A localized initial disturbance for an unstable system may not only grow with time as discussed in the previous Section, but also be amplified as it propagates and/or spreads in space. Therefore a study of the space-time evolution of an initially small disturbance is essential for the understanding of the instability process. It is thus necessary to investigate both absolute and convective instability, as shown by Briggs [16] and Bers [17]. The absolute instability is determined by using a convenient mesh-searching technique [26].

3.2.1 Pseudo-absolute instability of sinuous mode

Similar to the temporal case, there also exists a critical gas Weber number of one, below which the sinuous mode of disturbance remains neutrally stable. Figure 7 shows the formation of the pinch-point singularity for the sinuous mode at the Weber number $We_g = 0.9$, Reynolds number $Re = 1$, density ratio $\varrho = 0.001$ and Mach number $Ma = 0$. It is seen that the two branches of solutions in the complex m plane, one from the upper ($m_i > 0$) and the other from the lower ($m_i < 0$) plane, approach each other and merge to form a pinch point at (m_0, Ω_0). According to Briggs [16] and Bers [17], this pinch point represents an absolute instability if $\Omega_{0,i} > 0$. Further calculations show that for any Reynolds number, density ratio and Mach number (up to $Ma < 1$), the pinch point is always fixed at $m_0 = (0, 0)$ and $\Omega_0 = (0, 0)$, if the gas Weber number is less than one. Thus, although the formation of the pinch point may suggest the existence of an absolute instability in the system, the gas sheet is neutrally stable under these flow conditions

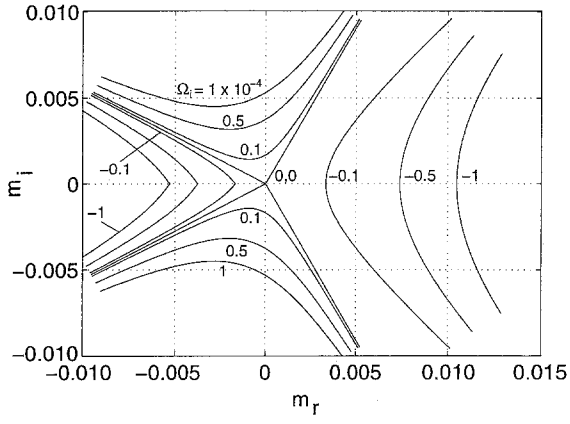

Fig. 7. Pseudo-absolute instability for sinuous mode. $We_g = 0.9$, $Re = 1$, $\varrho = 0.001$ and $Ma = 0$

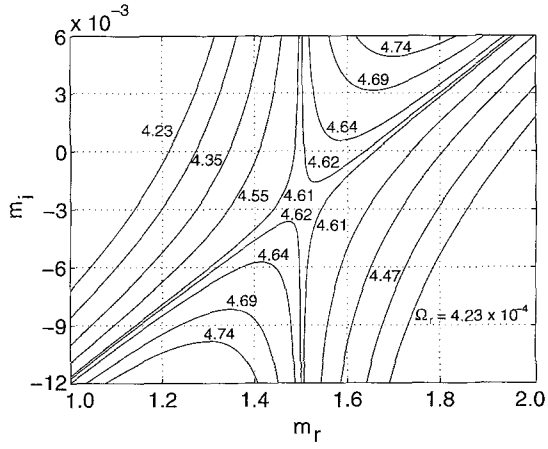

Fig. 8. Pinch point formation for sinuous mode. $We_g = 3.0$, $Re = 100$, $\varrho = 0.001$ and $Ma = 0$

because $\Omega_{0,i} = 0$. This result is similar to the instability of a plane liquid sheet subjected to sinuous disturbances with liquid Weber number less than one [18], [19], and, following Lin et al. [18], this neutral instability is termed as pseudo-absolute instability.

3.2.2 Absolute instability

Figure 8 shows the pinch point formation for the sinuous mode of disturbance at a gas Weber number $We_g = 3$, Reynolds number $Re = 100$, density ratio $\varrho = 0.001$ and $Ma = 0$. From Fig. 8 it is clear that the two branches of m_0, from the upper and lower plane respectively, merge to the pinch point $m_0 \approx (1.504, -2.8 \times 10^{-3})$ and $\Omega_0 \approx (4.62 \times 10^{-4}, 1.41 \times 10^{-2})$. Hence, this point represents absolute instability of the gas sheet with the absolutely unstable wave spreading in the direction of flow at a spatial growth rate of $m_{0,i} = -2.8 \times 10^{-3}$, and at a fixed spatial location the wave amplitude increases with time at a temporal rate of $\Omega_{0,i} = 1.41 \times 10^{-2}$.

On the other hand, if $\Omega_{0,i}$ is negative at a pinch point, then the absolute instability disappears and convective instability occurs [16], [17]. Thus the condition $\Omega_{0,i} = 0$ indicates the inception of the convective instability. For a liquid jet in surrounding gas medium, it is shown [26]–[29] that for a given Reynolds number and density ratio there exists a maximum Weber number, referred to as the critical Weber number, below which $\Omega_{0,i} > 0$, indicating the occurrence of absolute instability, and above which $\Omega_{0,i} < 0$, implying the existence of convective instability. However, for the present problem of gas sheets in a liquid medium, it is found that for both the varicose and the sinuous mode in the unstable range, i.e., $We_g > 1$ for the sinuous and $We_g > 0$ for the varicose mode, there is no flow condition for which $\Omega_{0,i} \leqq 0$. This suggests that there does not exist any convective instability for gas sheets. Thus, unlike the instability of a plane liquid sheet where only convective instability exists [18], [19] and a cylindrical liquid jet for which both absolute and convective instability are possible depending on the flow conditions [26]–[29], a gas sheet is absolutely unstable at any flow condition. An absolutely unstable gas sheet has two components of instability growth rate, temporal growth rate $\Omega_{0,i}$ and spatial growth rate $m_{o,i}$, which will be presented in the following Section.

3.2.3 Temporal growth rate of absolute instability

Generally the temporal part of absolute instability growth rate is increased by increased density ratio, reduced surface tension and reduced liquid viscosity for both sinuous and varicose modes of disturbances. A typical set of results is shown in Fig. 9 for the effect of liquid viscosity on the

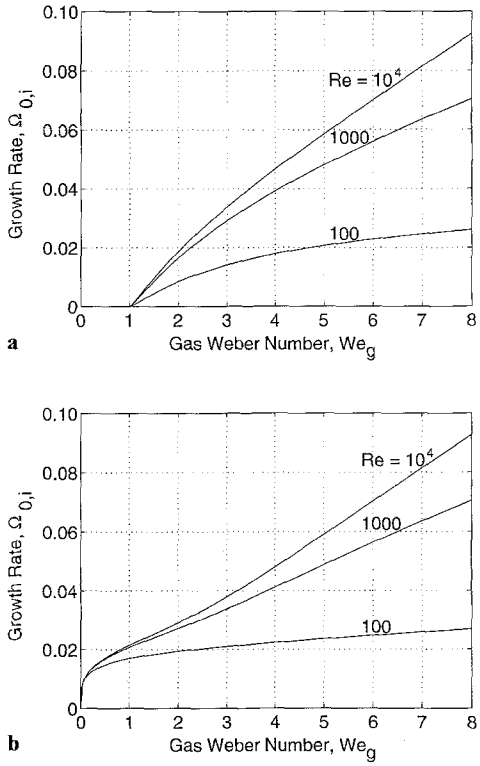

Fig. 9. Dimensionless temporal growth rate of absolute instability vs. gas Weber number for various Reynolds numbers. $\varrho = 0.001$ and Ma = 0. **a** Sinuous mode, **b** varicose mode

temporal growth rate of the absolute instability for both sinuous and varicose mode. It is seen that the temporal part of the growth rate increases with the Weber number, indicating that surface tension has a stabilizing effect, while gas inertial effect enhances the absolute instability. It is also seen in Fig. 9 that for any gas Weber number the growth rate increases with the Reynolds number. Thus, unlike the temporal instability of plane gas sheets where viscosity plays a dual role of stabilization and destabilization for the sinuous mode of disturbances at low Weber numbers [22], liquid viscosity always acts as an instability inhibitor for the temporal growth rate of absolute instability, no matter how small the Weber and Reynolds numbers may be. Further numerical calculations indicate that Fig. 9 well represents the viscous effect for any gas density ratio and Mach number.

Shown in Fig. 10 is a comparison between the temporal growth rate of absolute instability of sinuous and varicose modes of disturbances for inviscid and viscous (Re = 100) liquid at a density ratio $\varrho = 0.001$ and a Mach number Ma = 0. It is clear that the varicose mode of disturbance has a larger growth rate for both inviscid and viscous surrounding liquid and thus dominates the instability process. However, at high Weber numbers, the growth rate of the sinuous mode approaches asymptotically that of the varicose mode, implying that at high Weber numbers both modes are almost equally important in controlling the instability process. However, for viscous liquids, the varicose mode has a higher growth rate than that of the sinuous mode over a wider range of gas Weber numbers ($We_g > 8$) as compared to inviscid liquids where the growth rates of the two modes are almost equal at a smaller Weber number ($We_g \approx 5.5$). The damping effect of liquid viscosity on the growth rate of both modes of disturbances is also evident in Fig. 10, especially at higher Weber numbers.

The gas compressibility effect on the temporal growth rate of absolute instability is shown in Fig. 11 for both the sinuous and the varicose mode of disturbances at the density ratio $\varrho = 0.1$,

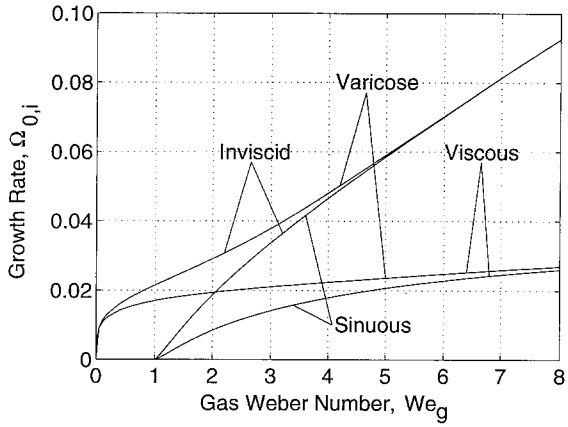

Fig. 10. Dimensionless temporal growth rate of absolute instability of sinuous and varicose mode for inviscid and viscous (Re = 100) liquid at $\varrho = 0.001$ and Ma = 0

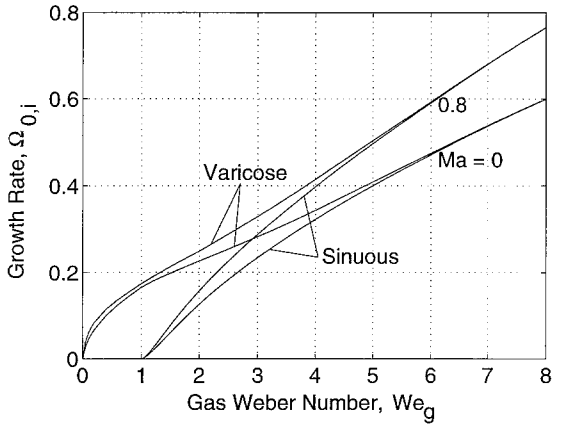

Fig. 11. Dimensionless temporal growth rate of absolute instability of sinuous and varicose mode for incompressible (Ma = 0) and compressible (Ma = 0.8) gas at $\varrho = 0.1$ and Re = 100

Reynolds number Re = 100 and Mach number of 0 and 0.8, respectively. Further results are given in Table 1 for Ma = 0, 0.4, 0.6 and 0.8, respectively. It is evident that the growth rates for both modes increase with the Mach number, indicating that gas compressibility enhances the temporal growth rate of absolute instability. Further, it is seen that the increment of growth rate with the Mach number becomes more significant at higher gas Weber numbers. Clearly, for both a compressible and an incompressible gas sheet, the temporal growth rate for the varicose mode is larger than that for the corresponding sinuous mode, indicating that the varicose mode governs the instability process for both incompressible and compressible gas sheets. However, as noted earlier, at large gas Weber numbers the temporal growth rate for the sinuous mode asymptotically reaches that for the varicose mode and both modes become equally important in the instability process. A comparison between Figs. 10 and 11 reveals that the temporal growth rate of absolute instability increases with the gas-to-liquid density ratio for both the sinuous and the varicose mode. This observation is valid for Ma up to one.

3.2.4 Spatial growth rate of absolute instability

Similar to the temporal part, the spatial part of the absolute instability growth rate is also increased by the density ratio of gas to liquid and reduced by liquid viscosity. On the other hand, surface tension and gas inertia, in the dimensionless form of gas Weber number We_g, has a complex effect on the spatial growth rate.

Table 1. Dimensionless temporal growth rate of absolute instability ($\Omega_{0,i}$). $\varrho = 0.1$ and Re = 100

We_g	$\Omega_{0,i}$ ($\times 10^{-1}$)							
	Sinuous				Varicose			
	Ma = 0	0.4	0.6	0.8	Ma = 0	0.4	0.6	0.8
0.1	0.0	0.0	0.0	0.0	0.0443	0.0522	0.0566	0.0593
1.0	0.0	0.0	0.0	0.0	1.6507	1.6670	1.7143	1.7363
2.0	1.2572	1.3448	1.4585	1.5695	2.2625	2.3798	2.4844	2.4901
3.0	2.3427	2.5045	2.7066	2.8795	2.8235	3.0023	3.1986	3.2929
4.0	3.2287	3.4539	3.7344	3.9777	3.4378	3.6721	3.9496	4.1496
5.0	4.0034	4.2871	4.6439	4.9710	4.0906	4.3788	4.7338	5.0389
6.0	4.7105	5.0499	5.4824	5.9043	4.7464	5.0879	5.5194	5.9305
7.0	5.3710	5.7643	6.2718	6.7965	5.3860	5.7802	6.2873	6.8067
8.0	5.9981	6.4435	7.0254	7.6579	6.0042	6.4500	7.0317	7.6617

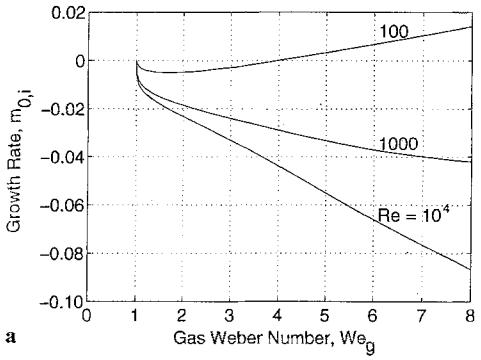

a

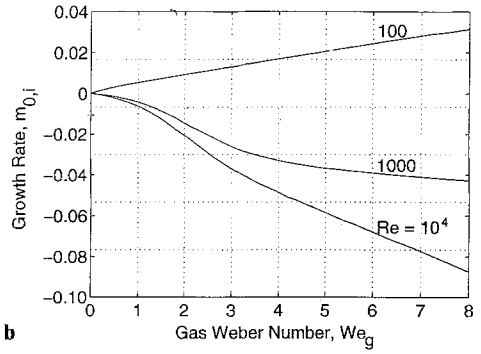

b

Fig. 12. Dimensionless spatial growth rate of absolute instability vs. gas Weber number for various Reynolds numbers. $\varrho = 0.001$ and Ma = 0. **a** Sinuous mode, **b** varicose mode

Figure 12 shows the spatial growth rate as a function of the gas Weber number for various Reynolds numbers with $\varrho = 0.001$ and Ma = 0. It is seen that at large Reynolds numbers (10^4 and 1000) the growth rate increases monotonically with the gas Weber number, suggesting that the surface tension effect inhibits and the gas inertial effect promotes the instability. However, for smaller Reynolds numbers the spatial growth rate for both sinuous and varicose mode increases with the gas Weber number first until reaching a maximum value, then it decreases, as shown in Fig. 12a for Re = 100. When the gas Weber number is increased further, eventually $m_{0,i}$ becomes positive at large Weber numbers, indicating that now the absolutely unstable disturbance decays spatially as it spreads downstream, although it is still amplified with time. This suggests that the gas Weber number has both a stabilizing and a destabilizing effect on the spatial growth rate, which clearly contrasts with the results of both the temporal instability and the temporal part of

absolute instability growth rate where the gas Weber number always enhances instability. For highly viscous liquids, the spatial growth rate $m_{0,i}$ would be positive for any value of the Weber number, just like the result for Re = 100 shown in Fig. 12 b. The above results also imply that viscous effects always reduce the spatial growth rate for both sinuous and varicose modes, and the reduction becomes more significant as the gas Weber number is increased, such that $m_{0,i}$ becomes positive first at high Weber numbers as the viscous effect is increased, and eventually it is positive for any Weber numbers when the Reynolds number is sufficiently small. Figure 12 also indicates that viscous effect is more significant for the varicose mode than for the sinuous mode.

The results presented in Fig. 12 further suggest the existence of a critical gas Weber number at which $m_{0,i} = 0$ for a given set of Reynolds numbers, density ratio and Mach number. Further numerical calculations indicate that out of the four dimensionless parameters, density ratio, gas Weber number, Reynolds number and Mach number, if any three are kept constant, there exists a critical value of the fourth parameter which marks the transition from spatially growing disturbance wave ($m_{0,i} < 0$) to spatially decaying disturbance wave ($m_{0,i} > 0$) or vice versa. A typical set of results for both the sinuous and the varicose mode of disturbances is presented in Table 2 where a critical Reynolds number, at which $m_{0,i} = 0$, is determined for a given density ratio $\varrho = 0.001$ and Mach number Ma = 0. For the given conditions, if the Reynolds number is less than the critical value given in Table 2, $m_{0,i}$ is positive indicating a spatially decaying wave. On the other hand, $m_{0,i}$ is negative if the Reynolds number is larger than the critical value, implying spatially growing waves. It is seen in Table 2 that the critical Reynolds number increases with the Weber number for sinuous disturbances and decreases for varicose disturbances. For $We_g \leqq 1$, as shown earlier, pseudo-absolute instability exists for the sinuous mode such that $m_{0,i}$ is always equal to zero for any Reynolds numbers. It should be pointed out that for both the sinuous and the varicose modes the temporal growth rate $\Omega_{0,i}$ is always positive, even though the spatial growth rate may be negative or positive, depending on the flow conditions. Physically it may be interpreted that although liquid viscosity always has a stabilizing effect on both temporal and spatial growth rate of absolute instability, for Reynolds numbers higher than the critical value, viscous effects being relatively small, disturbance waves grow in amplitude both with downstream distance and with time. On the other hand, if the Reynolds number is less than the

Table 2. Critical Reynolds numbers at density ratio $\varrho = 0.001$, Ma = 0

Gas Weber number We_g	Critical Reynolds number, Re_c	
	Sinuous mode	Variscose mode
0.4	–	338.0
0.8	–	279.0
1.2	19.5	246.5
1.6	31.0	225.0
2.0	42.0	209.5
2.4	52.8	197.5
2.8	64.2	188.0
3.2	76.3	182.0
3.6	88.9	178.0
4.0	101.9	176.0
4.4	115.5	176.5
4.8	129.5	179.0
5.2	143.0	183.5
5.6	157.0	189.5
6.0	171.0	197.0

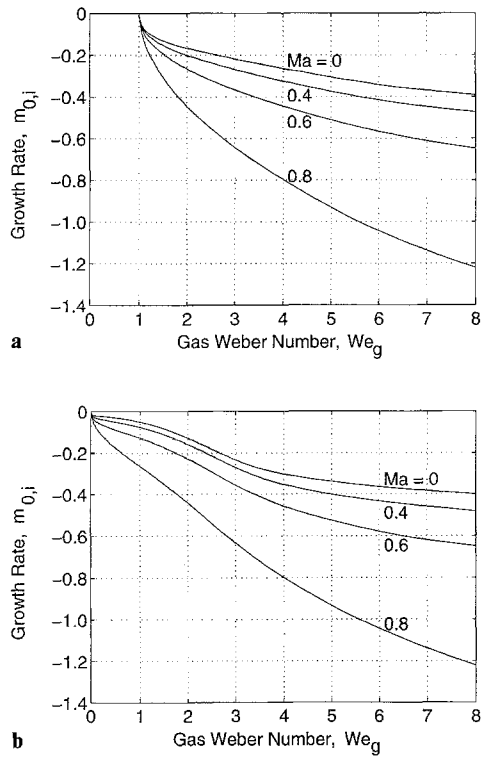

Fig. 13. Dimensionless spatial growth rate of absolute instability vs. gas Weber number for various Mach numbers. Re = 100 and $\varrho = 0.1$. **a** Sinuous mode, **b** varicose mode

critical value, viscosity damps out any spatially growing wave such that at any given time the disturbance amplitude decreases in the downstream direction. However, at any fixed spatial location disturbance the amplitude grows with time until the continuous gas sheet breaks up eventually.

Similar to the temporal growth rate discussed in the earlier Section, the gas compressibility also has a destabilizing effect on the spatial growth rate. In Fig. 13 is shown the effect of the Mach number on the spatial growth rate of absolute instability for the density ratio $\varrho = 0.1$ and the Reynolds number Re = 100. Clearly, the spatial growth rate for both the sinuous and the varicose mode increases significantly with the Mach number, especially at high gas Weber numbers. Further numerical calculations indicate that Fig. 13 is representative of the compressibility effect on the spatial growth rate for any density ratio and Reynolds number. Thus, it may be concluded that the compressibility effect enhances the absolute instability as a whole. Further, a comparison between Figs. 12 and 13 indicates that the gas-to-liquid density ratio increases the spatial growth rate, thus promoting the instability process.

3.2.5 Wave velocity

Wave velocity is enhanced by increased density ratio and gas compressibility effect and reduced by liquid viscosity for both the sinuous and the varicose mode of disturbances. The gas Weber number, on the other hand, has a more complex effect. A typical set of results is shown in Fig. 14 for the sinuous and the varicose mode of disturbances at the density ratio $\varrho = 0.1$ and Reynolds number Re = 100. For the sinuous mode of disturbances, wave velocity initially increases with the gas Weber number until it reaches a peak value and then decreases slowly with the Weber number. Whereas for varicose mode, the wave velocity decreases monotonically with the Weber

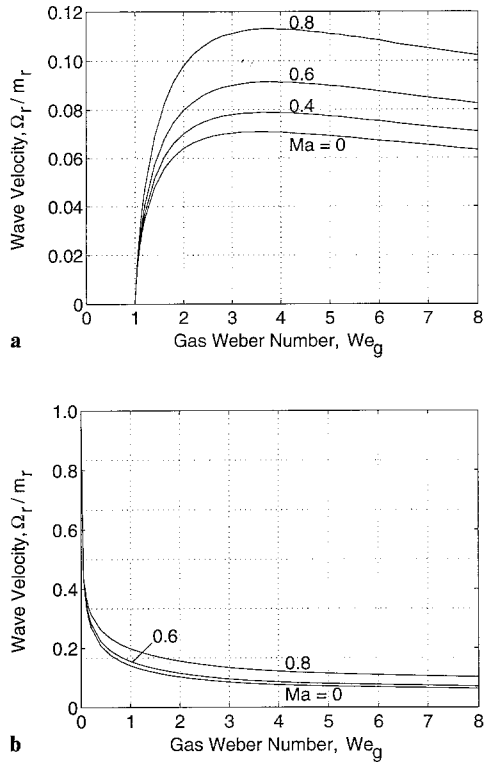

Fig. 14. Dimensionless wave velocity vs. gas Weber number for various Mach numbers. Re = 100 and $\varrho = 0.1$. **a** Sinuous mode, **b** varicose mode

number. It is also clear that the wave velocity increases with the Mach number for both modes of disturbances, although at small gas Weber numbers the increment is small. Evidently the wave velocity for compressible gas sheets is not significantly small compared to the gas sheet velocity, in contrast with the incompressible case at the mode of maximum instability [22].

4 Conclusion

The temporal, absolute and convective instability of a plane compressible gas sheet in a quiescent viscous liquid medium of infinite expanse has been investigated. It is found that two unstable modes of disturbances, sinuous and varicose, exist in the instability process, and temporal and absolute instability occur whereas convective instability is absent for such a gas sheet.

For temporal instability, both the gas compressibility and the liquid viscosity increase the instability limit for both unstable modes. Gas compressibility always enhances the disturbance growth rate though the increase is small at low Weber numbers and low Mach numbers. For sinuous mode, there exists a critical Weber number of unity below which it is always stable. The maximum growth rate, dominant wave number and wave velocity for both modes all increase with the Mach number.

An analysis of space-time evolution of disturbances shows that for the sinuous mode of disturbance there exists a critical gas Weber number of one, below which pseudo-absolute instability occurs. Whereas only absolute instability exists for the sinuous mode above this critical value of one and for varicose mode at any gas Weber numbers. In contrast with the instability of plane liquid sheets and circular liquid jets, there does not exist any convective

instability for plane gas sheets. It is further found that, depending on the flow condition, the absolutely unstable disturbance may be spatially growing or decaying, but it is always temporally growing. Gas compressibility enhances, while liquid viscosity reduces both the temporal and the spatial part of the absolute instability growth rate. Surface tension always inhibits, while gas inertia enhances the temporal growth rate of absolute instability. On the other hand, surface tension and gas inertia have a complex dual effect of enhancing and suppressing the spatial growth rate of absolute instability.

For both temporal and absolute instability, the varicose mode has a higher growth rate than the coresponding sinuous mode and thus controls the overall instability process of plane gas sheets for low and intermediate Weber numbers. At large Weber numbers, the growth rates of both modes are almost equal and thus are equally important in the instability process.

Acknowledgement

This work is supported by the Natural Sciences and Engineering Research Council of Canada.

References

[1] Clift, R., Grace, J. R., Weber, M. E.: Bubbles, drops and particles. New York: Academic Press 1978.
[2] Leonard III, J. W.: Coal preparation, 5th ed. Littleton: Society for Mining, Metallurgy and Exploration Inc., 1991.
[3] Yianatos, J. B., Laplante, A. R., Finch, J. A.: Estimation of local holdup in the bubbling and froth zones of a gas-liquid column. Chem. Eng. Sci. **40,** 1965–1968 (1985).
[4] Blevins, R. D.: Applied fluid dynamics handbook. Malabar: Krieger 1992.
[5] Topham, D. R.: Hydrodynamics of an oil well blowout. Beaufort Sea Tech. Report, Inst. Ocean Sci., Sidney B. C., **33** (1975).
[6] Milgram, J. H.: Mean flow in round bubble plumes. J. Fluid Mech. **133,** 345–376 (1983).
[7] Asaeda, T., Imberger, J.: Structure of bubble plumes in stratified environments. J. Fluid Mech. **249,** 35–57 (1993).
[8] Giffen, E., Muraszew, A.: The atomization of liquid fuels. New York: Wiley 1953.
[9] Lefebvre, A. H.: Gas turbine combustion. New York: Hemisphere 1983.
[10] Lefebvre, A. H.: Atomization and sprays. New York: Hemisphere 1989.
[11] Masters, K.: Spray drying handbook, 4th ed. New York: Wiley 1985.
[12] Squire, H. B.: Investigation of the instability of a moving liquid film. Br. J. Appl. Phys. **4,** 167–169 (1953).
[13] York, J. L., Stubbs, H. E., Tek, M. R.: The mechanism of disintegration of liquid sheets. Trans. ASME **75,** 1279–1286 (1953).
[14] Hagerty, W. W., Shea, J. F.: A study of the stability of plane fluid sheets. J. Appl. Mech. **22,** 509–514 (1955).
[15] Li, X., Tankin, R. S.: On the temporal instability of a two-dimensional viscous liquid sheet. J. Fluid Mech. **226,** 425–443 (1991).
[16] Briggs, R. J.: Electron stream interaction with plasma. Cambridge: MIT Press 1964.
[17] Bers, A.: Space-time evolution of plasma instability – absolute and convective. In: Handbook of plasma physics, (Rosenbluth, M. N., Sagdeev, R. Z., eds.) Vol. 1, pp. 452–517. Amsterdam: North-Holland 1983.
[18] Lin, S. P., Lian, Z. W., Creighton, B. J.: Absolute and convective instability of a liquid sheet. J. Fluid Mech. **220,** 673–689 (1990).
[19] Li, X.: Spatial instability of plane liquid sheets. Chem. Eng. Sci. **48,** 2973–2981 (1993).
[20] Ibrahim, E. A.: Spatial instability of a viscous liquid sheet. AIAA J. Prop. Power **11,** 146–152 (1995).
[21] Li, X.: Spatial instability of plane liquid sheets. In: Mixed-flow hydrodynamics, (Cheremisinoff, N. P. ed.). Advances in Engineering Fluid Mechanics series, Chap. 7, pp. 145–164. Houston: Gulf Publishing Co. 1996.

[22] Li, X., Bhunia, A.: Temporal instability of plane gas sheets in a viscous liquid medium. Phys. Fluids **8,** 103–111 (1996).
[23] Bhunia, A.: Instability of plane gas sheets in viscous liquid medium. M. A. Sci. Thesis, University of Victoria, Victoria, B. C., 1995.
[24] Lin, S. P., Ibrahim, E. A.: Stability of a viscous liquid jet surrounded by a viscous gas in a vertical pipe. J. Fluid Mech. **218,** 641–658 (1990).
[25] Muller, D. E.: A method for solving algebraic equations using an automatic computer. Math. Tables Aid Comp. **10,** 208–215 (1956).
[26] Li, X., Shen, J.: Absolute and convective instability of a cylindrical liquid jet in a co-flowing gas stream. Atom. Sprays (accepted for publication).
[27] Leib, S. J., Goldstein, M. E.: The generation of capillary instabilities on a liquid jet. J. Fluid Mech. **168,** 479–500 (1986).
[28] Leib, S. J., Goldstein, M. E.: Convective and absolute instability of a viscous liquid jet. Phys. Fluids **A 29,** 952–954 (1986).
[29] Lin, S. P., Lian, Z. W.: Absolute instability of a liquid jet in a gas. Phys. Fluids **A 32,** 490–499 (1989).

Authors' address: Assoc. Prof. X. Li and A. Bhunia, Department of Mechanical Engineering, University of Victoria, Victoria, B. C. V8W 3P6, Canada